

Doping change and distortion effect on double-exchange ferromagnetism

Phan Van-Nham and Tran Minh-Tien

Institute of Physics and Electronics, VAST, P.O. Box 429, Boho, 10000 Hanoi, Vietnam.

Doping change and distortion effect on the double-exchange ferromagnetism are studied within a simplified double-exchange model. The presence of distortion is modelled by introducing the Falicov-Kimball interaction between itinerant electrons and classical variables. By employing the dynamical mean-field theory the charge and spin susceptibility are exactly calculated. It is found that there is a competition between the double-exchange induced ferromagnetism and disorder-order transition. At low temperature various long-range order phases such as charge ordered and segregated phases coexist with ferromagnetism depending on doping and distortion. A rich phase diagram is obtained.

PACS numbers: 71.27.+a, 71.28.+d, 75.30.-m

I. INTRODUCTION

The discovery of colossal magnetoresistance in doped manganites^{1,2} has renewed interest in the ferromagnetism induced by the double-exchange (DE) mechanism.³ The main feature of the DE mechanism is a cooperative effect where electron hopping favors ferromagnetic (FM) ordering of localized spins via the FM Hund coupling, and vice versa, the presence of the FM order facilitates the electron hopping. The occurrence of metallic FM state in doped manganites $R_{1-x}A_xMnO_3$ (where R is a trivalent rare-earth element and A is a divalent alkaline ion) was qualitatively explained by the DE mechanism.⁴ The physically relevant electrons in these compounds are those from Mn 3d levels which are split by the cubic crystalline field into triply degenerate t_{2g} levels and doubly degenerate e_g levels. Electrons of e_g levels are able to hop between Mn sites and form the conduction band, while electrons of t_{2g} levels are localized. Conduction electrons and localized spins are correlated by the DE mechanism which leads to the appearance of the metallic FM phase. The DE model became the starting point toward comprehensive understanding of the properties of doped manganites.

Experiments have observed in doped manganites a very rich phase diagram, which involves phases with spin, charge and orbital orders.¹ For the undoped case ($x = 0$) all Mn ions are Mn^{3+} and are expected to induce a Jahn-Teller (JT) distortion. For the other extreme doping ($x = 1$) all Mn ions are Mn^{4+} and do not couple to the JT distortion. In the regime of intermediate doping, two valence ions Mn^{3+} and Mn^{4+} are simultaneously present. The presence of two valence ions may lead to a static mixed valence Mn^{3+}/Mn^{4+} configuration, in particular, to an alternation charge-ordered (CO) state of Mn^{3+}/Mn^{4+} ions for appropriate dopings. This is the conventional view, for which there are abundant experimental and theoretical supports.^{1,2} In particular, recently a CO-FM state has been observed.⁵ However, there are several experiments which challenge the conventional view. Several x-ray absorption^{6,7,8,9} and neutron diffraction studies¹⁰ revealed pictures that do not match with the static mixture of Mn^{3+} and Mn^{4+} ions.

One suggests that all Mn ions have the same valence and result into the Zener-polaron state.^{11,12} However, very recent experiment⁸ observed the presence of two types of Mn sites with different local geometric structures. One of the types of Mn sites is surrounded by a tetragonal-distorted oxygen octahedron, whereas the other has a regular octahedral environment. As a result a charge segregation state was deduced. With the motivation of the experimental observations⁸ we model the presence of the two types of Mn sites by incorporating the Falicov-Kimball (FK) model.¹³ The FK model was initially introduced as a statistical model for metal-insulator transition.¹³ Later it was also applied to valence change transitions in intermetallic compounds.^{14,15} Within the FK model the presence of two types of Mn sites is mapped to a classical variable which only accept two values (for instance, 1 and 0). The energy difference of these sites is mapped into the interaction strength of the FK model. Indeed, the sites surrounded by tetragonal-distorted octahedron have induced the JT distortion. As a consequence the energy levels of the distorted Mn sites are split. The FK model can describe a charge ordered phase as well as a charge segregated phase.¹⁶ In particular, the model can exhibit the checkerboard CO state in appropriate conditions. The checkerboard CO state is truly a mixed-valence state. The segregated state is a phase-separated mixture of two full uniform configurations.^{17,18,19,20} In such the way, at low temperature the FK model could establish various phases with different charge configurations which may correspond to the experimental observations.⁸

However, the FK model alone cannot describe the DE induced FM state which was also observed in doped manganites. Therefore we incorporate the FK model into the DE model in order to study both the charge ordered phases and the ferromagnetism upon doping. The combined model has previously been considered in the context of order-disorder change of the A-site substitution.²¹ In the previous study²¹ only the checkerboard CO and FM state are considered in the limit of infinite value of the Hund coupling. In this paper we study all possible ordered phases of the combined model in whole range of doping and interaction. In order to detect the

phase transition we study the static charge and spin response of system within the dynamical-mean field theory (DMFT).²² The DMFT has been widely used for investigating strongly correlated electron systems. Within the DMFT the static charge and spin correlation function are calculated explicitly. We find that the system exhibits a rich phase diagram which includes various charge ordered phases coexisting with ferromagnetism. In particular, the checkerboard CO state or the segregated state can coexist with the FM state. The combined model can also serve as a model for studying the problem of order-disorder A-site substitution²¹ or the problem of orbital ordering in doped manganites.^{23,24}

The present paper is organized as follows: In Sec. II we present the combined FK and DE model and its DMFT solutions. In Sec. III the charge and spin correlation functions are calculated explicitly. The numerical results and discussions are presented in Sec. IV. The final section is conclusion and remark.

II. MODEL AND DYNAMICAL MEAN-FIELD THEORY

The combined FK and DE model in our study is described by the following Hamiltonian

$$H = -t \sum_{\langle ij \rangle, \sigma} c_{i\sigma}^\dagger c_{j\sigma} - \mu \sum_{i\sigma} c_{i\sigma}^\dagger c_{i\sigma} - 2J_H \sum_i S_i^z s_i^z + U \sum_{i\sigma} n_{i\sigma} w_i + E_w \sum_i w_i, \quad (1)$$

where $c_{i\sigma}^\dagger$ ($c_{i\sigma}$) is the creation (annihilation) operator for an itinerant electron with spin σ at lattice site i . The first term in Hamiltonian (1) represents the hoping of itinerant electrons between the nearest neighbor sites. t is the hoping integral and is scaled with the spatial dimension d as $t = t^*/(2\sqrt{d})$.²⁶ In the following we will take $t^* = 1$ as the unit of energy. S_i^z is the z component of localized spin at lattice site i . For simplicity, it takes two values $-1, 1$. $s_i^z = (c_{i\uparrow}^\dagger c_{i\uparrow} - c_{i\downarrow}^\dagger c_{i\downarrow})/2$ is the z component of itinerant electron spin. w_i is a classical variable that assumes the value $1(0)$ if site i is surrounded by distorted (regular) octahedron. U is the interaction strength and is mapped into the difference in the level energy of these sites. The expectation value $\rho_w = \sum_i \langle w_i \rangle / N$, (N is the number of lattice sites), corresponds to the concentration of distorted sites. The chemical potential μ controls the doping $n_e = \sum_{i\sigma} \langle n_{i\sigma} \rangle / N$, while E_w controls the fraction of distorted sites. The condition $n_e + \rho_w = 1$ is used to determine E_w for each doping n_e . The first three terms in Hamiltonian (1) describe a simplified DE model which contains only the Ising-type interaction between the itinerant and localized electron spins. The simplification does not allow any spin-flip processes, which can be important at low temperature where spin-wave excitations may govern the thermodynamics of the system. However, in the DE processes spins

of itinerant electrons align ferromagnetically with the localized spins, hence the Ising part of the Hund coupling plays a dominant role. Within the DMFT the simplified DE model is equivalent to the DE model with classical localized spins in the disordered paramagnetic phase.⁴ The transport quantities calculated within the simplified model capture essential features of the full DE model.²⁷ The simplified DE model has also previously been used in the study of doped manganites.²⁸ The last two terms in Hamiltonian (1) take into account the energy difference of Mn sites. They together with the hoping term form the FK model.¹³ Several authors have also constructed the combined model to study the properties of manganites in different contexts and regimes.^{21,23,24,25} Ferrari *et al.* used the combined model to study the metallic FM phase of the two orbital DE model.²⁴ Recently, Ramakrishnan *et al.* basically used the combined model to construct a two band model of localized polaronic and broad band states.²⁵ They used the DMFT to calculate transport quantities and explained the metal insulator transition and the colossal magnetoresistance in doped manganites.²⁵

We solve the combined model (1) by the DMFT.²² The DMFT is based on the infinite dimension limit. In the infinite dimension limit the self-energy is pure local and does not depend on momentum. The Green function of itinerant electrons with spin σ satisfies the Dyson equation

$$G_\sigma(\mathbf{k}, i\omega_n) = \frac{1}{i\omega_n - \epsilon(\mathbf{k}) + \mu - \Sigma_\sigma(i\omega_n)}, \quad (2)$$

where $\epsilon(\mathbf{k}) = -2t \sum_{i=1,d} \cos(k_i)$ is the dispersion of free itinerant electrons on a hypercubic lattice, and $\Sigma_\sigma(i\omega_n)$ is the self energy which depends only on frequency. The self energy is determined by solving an effective single-site problem. The action for this effective problem is

$$S_{\text{eff}} = - \int_0^\beta d\tau \int_0^\beta d\tau' \sum_\sigma c_\sigma^\dagger(\tau) \mathcal{G}_\sigma^{-1}(\tau - \tau') c_\sigma(\tau') - \int_0^\beta d\tau \sum_\sigma [J_H S^z \sigma + \mu - U w] c_\sigma^\dagger(\tau) c_\sigma(\tau) + \beta E_w w, \quad (3)$$

where $\mathcal{G}_\sigma(\tau - \tau')$ is the Green function of the effective medium. It plays as the bare Green function of the effective problem. The local Green function also satisfies the Dyson equation

$$G_\sigma^{-1}(i\omega_n) = \mathcal{G}_\sigma^{-1}(i\omega_n) - \Sigma_\sigma(i\omega_n), \quad (4)$$

where $\mathcal{G}_\sigma(i\omega_n)$ is the Fourier transform of $\mathcal{G}_\sigma(\tau)$. The local Green function $G_\sigma(i\omega_n)$ of the effective single-site problem is solely determined by the partition function

$$G_\sigma(i\omega_n) = \frac{\delta \ln \mathcal{Z}_{\text{eff}}}{\delta \mathcal{G}_\sigma^{-1}(i\omega_n)}, \quad (5)$$

where Z_{eff} is the partition function of the effective problem (3). The self-consistent condition of the DMFT requires that the local Green function $G_\sigma(i\omega_n)$ obtained

within the effective problem must coincide with the local Green function of the original lattice, i.e.,

$$G_\sigma(i\omega_n) = \frac{1}{N} \sum_{\mathbf{k}} G_\sigma(\mathbf{k}, i\omega_n) = \int d\epsilon \rho(\epsilon) \frac{1}{i\omega_n - \epsilon + \mu - \Sigma_\sigma(i\omega_n)}, \quad (6)$$

where $\rho(\epsilon)$ is the density of state (DOS) of noninteracting itinerant electrons. In the infinite dimension limit of hypercubic lattices it has the form $\rho(\epsilon) = \exp(-\epsilon^2/(t^*)^2)/\sqrt{\pi}t^*$. Eqs. (4), (5) and (6) form the self-consistent equations for determining the self-energy, and hence, also the Green function of the original lattice. Within the effective single-site problem, the partition function is

$$\mathcal{Z}_{\text{eff}} = \text{Tr} \int Dc_\sigma^\dagger Dc_\sigma e^{-S_{\text{eff}}}, \quad (7)$$

where the trace is taken over S^z and w . This partition function can be calculated exactly. It is similar to solve the FK model within the DMFT.²⁹ We obtain

$$\mathcal{Z}_{\text{eff}} = 2 \sum_{\alpha=0,1} \sum_{s=\pm 1} \exp \left[-\beta E_w \alpha + \sum_{n\sigma} \ln \frac{Z_\sigma(i\omega_n) + \sigma s J_H - \alpha U}{i\omega_n} \right], \quad (8)$$

where $Z_\sigma(i\omega_n) \equiv \mathcal{G}_\sigma^{-1}(i\omega_n)$. Using Eq. (5) we obtain the local Green function

$$G_\sigma(i\omega_n) = \sum_{\alpha s} \frac{W_{\alpha s}}{Z_\sigma(i\omega_n) + \sigma s J_H - \alpha U}, \quad (9)$$

where the weight factors $W_{\alpha s}$ are

$$W_{\alpha s} = \frac{2}{\mathcal{Z}_{\text{eff}}} \exp \left[-\beta E_w \alpha + \sum_{n\sigma} \ln \frac{Z_\sigma(i\omega_n) + \sigma s J_H - \alpha U}{i\omega_n} \right] \quad (10)$$

with $\alpha = 0, 1$ and $s = \pm 1$. Note that the weight factors $W_{\alpha s}$ are not simply a number. They are functionals of the local Green function. This is an important feature of the DMFT that gives nontrivial contributions to the response functions of the system.²⁹ In the paramagnetic phase $Z_\uparrow(i\omega_n) = Z_\downarrow(i\omega_n)$, hence $W_{\alpha s} = W_{\alpha, -s}$ that leads the Green function (9) and the self energy are independent of spin indeces, as expected. The value of E_w is adjusted that the concentration ρ_w fulfills $n_e + \rho_w = 1$ for each doping n_e . One can show that

$$\rho_w = \sum_{s=\pm 1} W_{1s}. \quad (11)$$

We use this equation to adjust the value of E_w . So far, we have obtained closed system of equations for determining the Green function of the system. The system of equations can be solved numerically by iterations.¹⁶

III. INSTABILITY OF HOMOGENEOUS PARAMAGNETIC PHASE

In order to detect the charge and spin ordered states which are established at low temperature we study the static charge and spin correlation function of itinerant electrons in disordered paramagnetic phase. The signal of a phase transition is a divergence of these correlation functions at a certain momentum. The charge (c) and spin (s) correlation function are defined as

$$\chi^{c(s)}(i, j) = \langle (\delta n_{i\uparrow} \pm \delta n_{i\downarrow})(\delta n_{j\uparrow} \pm \delta n_{j\downarrow}) \rangle, \quad (12)$$

where $\delta n_{i\sigma} = n_{i\sigma} - \langle n_{i\sigma} \rangle$. These correlation functions can be expressed as

$$\chi^{c(s)}(i, j) = \sum_{\sigma\sigma'} \chi_{\sigma\sigma'}(i, j) \xi_\sigma \xi_{\sigma'}, \quad (13)$$

where $\chi_{\sigma\sigma'}(i, j) = \langle \delta n_{i\sigma} \delta n_{j\sigma'} \rangle$, and $\xi_\sigma = 1$ for the charge correlation function and $\xi_\sigma = \sigma$ for the spin correlation function. In order to calculate the static correlation functions, one has to introduce external fields $h_{i\sigma}$ which couple to $n_{i\sigma}$ into the Hamiltonian. The correlation functions $\chi_{\sigma\sigma'}(i, j)$ are obtained by differentiating the Green function with respect to the external fields and then taking the zero limit of the fields,²⁹ i.e.,

$$\chi_{\sigma\sigma'}(i, j) = -T^2 \sum_n \frac{dG_{ii,\sigma}(i\omega_n)}{dh_{j\sigma'}} \Big|_{\{h\}=0}. \quad (14)$$

Following the standard technique,^{16,29} one can express the charge and spin correlation function in the terms of the charge and spin susceptibility $\chi^{c(s)}(\mathbf{q}, i\omega_n)$

$$\chi^{c(s)}(\mathbf{q}) = -T^2 \sum_n \chi^{c(s)}(\mathbf{q}, i\omega_n), \quad (15)$$

where $\chi^{c(s)}(\mathbf{q})$ is the static charge (spin) correlation function in momentum space. From the definition of charge and spin correlation function (13) and relation (14), we obtain

$$\chi^{c(s)}(\mathbf{q}, i\omega_n) = 2\chi_0(\mathbf{q}, i\omega_n) + \chi_0(\mathbf{q}, i\omega_n) \frac{1}{2} \sum_{\nu\sigma\sigma'} \frac{d\Sigma_\sigma(i\omega_n)}{dG_{\sigma'}(i\omega_\nu)} \xi_\sigma \xi_{\sigma'} \chi^{c(s)}(\mathbf{q}, i\omega_\nu), \quad (16)$$

where $\chi_0(\mathbf{q}, i\omega_n) = \sum_{\mathbf{k}} G_\sigma(\mathbf{k} + \mathbf{q}, i\omega_n) G_\sigma(\mathbf{k}, i\omega_n)$ is the bare particle-hole susceptibility. Here we have used the fact that in the paramagnetic phase

$$d\Sigma_\uparrow(i\omega_n)/dG_\uparrow(i\omega_n) = d\Sigma_\downarrow(i\omega_n)/dG_\downarrow(i\omega_n), \quad (17)$$

$$d\Sigma_\uparrow(i\omega_n)/dG_\downarrow(i\omega_n) = d\Sigma_\downarrow(i\omega_n)/dG_\uparrow(i\omega_n). \quad (18)$$

From Eqs. (4) and (9), we obtain the self-energy $\Sigma_\sigma(i\omega_n)$ as a functional of $G_\sigma(i\omega_n)$ and $W_{\alpha s}$, hence its full deriva-

ties in Eq. (16) are expressed through its partial derivatives. We obtain

$$\begin{aligned} \frac{d\Sigma_\sigma(i\omega_n)}{dG_{\sigma'}(i\omega_\nu)} &= \delta_{n\nu}\delta_{\sigma\sigma'}\left(\frac{\partial\Sigma_\sigma(i\omega_n)}{\partial G_{\sigma'}(i\omega_n)}\right)_W \\ &+ \sum_{\alpha s}\left(\frac{\partial\Sigma_\sigma(i\omega_n)}{\partial W_{\alpha s}}\right)_{G, W_{\overline{\alpha s}}}\frac{\delta W_{\alpha s}}{\delta G_{\sigma'}(i\omega_n)}, \end{aligned} \quad (19)$$

where $W_{\overline{\alpha s}}$ means all weight factors W except $W_{\alpha s}$. Substituting (19) into Eq. (16) we arrive at

$$\chi^{c(s)}(\mathbf{q}, i\omega_n) = \frac{2 + \frac{1}{2}\sum_{\alpha s\sigma}\left(\frac{\partial\Sigma_\sigma(i\omega_n)}{\partial W_{\alpha s}}\right)_{G, W_{\overline{\alpha s}}}\xi_\sigma\xi_s\gamma_{\alpha s}(\mathbf{q})}{[\chi_0(\mathbf{q}, i\omega_n)]^{-1} - \frac{1}{2}\sum_\sigma\left(\frac{\partial\Sigma_\sigma(i\omega_n)}{\partial G_\sigma}\right)_W}, \quad (20)$$

where the matrix elements of $\hat{\gamma}(\mathbf{q})$ are

$$\gamma_{\alpha s}(\mathbf{q}) = \sum_{\nu\sigma'}\left(\frac{\delta W_{\alpha s}}{\delta G_{\sigma'}(i\omega_\nu)}\right)\xi_s\xi_{\sigma'}\chi^{c(s)}(\mathbf{q}, i\omega_\nu). \quad (21)$$

The functional derivative of $W_{\alpha s}$ in the above equation can explicitly be expressed through the derivatives of $W_{\alpha s}$ with respect to $Z_\sigma(i\omega_n)$ and the partial derivatives of the self energy $\Sigma_\sigma(i\omega_n)$.²⁹ Substituting (20) into (21) and performing some algebraic calculations we obtain the following matrix equation

$$\hat{Q}(\mathbf{q})\hat{\gamma}(\mathbf{q}) = \hat{P}(\mathbf{q}), \quad (22)$$

where the matrixes $\hat{Q}(\mathbf{q})$, $\hat{P}(\mathbf{q})$ have the following elements

$$\begin{aligned} Q_{\alpha s, \alpha' s'}(\mathbf{q}) &= \delta_{\alpha s, \alpha' s'} + \\ &\sum_{n\sigma\sigma'}\left\{R_{\alpha s, \sigma}(i\omega_n)S_{\sigma', \alpha' s'}(i\omega_n)\left(\frac{1}{2} - \delta_{\sigma\sigma'}\right) - \frac{1}{2}\frac{R_{\alpha s, \sigma}(i\omega_n)S_{\sigma', \alpha' s'}(i\omega_n)\eta_n(\mathbf{q})G(i\omega_n)}{1 - G^2(i\omega_n)\left(\frac{\partial\Sigma(i\omega_n)}{\partial G(i\omega_n)}\right)_W + \eta_n(\mathbf{q})G(i\omega_n)}\right\}, \end{aligned} \quad (23)$$

$$P_{\alpha s}(\mathbf{q}) = 2\sum_{n\sigma}\frac{R_{\alpha s, \sigma}(i\omega_n)\left(G^2(i\omega_n)\left(\frac{\partial\Sigma(i\omega_n)}{\partial G(i\omega_n)}\right)_W - 1\right)}{1 - G^2(i\omega_n)\left(\frac{\partial\Sigma(i\omega_n)}{\partial G(i\omega_n)}\right)_W + \eta_n(\mathbf{q})G(i\omega_n)}. \quad (24)$$

Here we have introduced the following notations

$$\begin{aligned} R_{\alpha s, \sigma}(i\omega_n) &= \frac{\partial W_{\alpha s}}{\partial Z_\sigma(i\omega_n)}\xi_s\xi_\sigma, \\ S_{\sigma, \alpha s}(i\omega_n) &= \frac{\partial\Sigma_\sigma(i\omega_n)}{\partial W_{\alpha s}}\xi_\sigma\xi_s, \end{aligned}$$

and $\eta_n(\mathbf{q}) = -G^{-1}(i\omega_n) + G(i\omega_n)\chi_0^{-1}(\mathbf{q}, i\omega_n)$. In Eqs. (23)-(24) the spin indices of the Green function and the self energy are omitted since they are in the paramagnetic phase. The derivatives in Eqs. (23)-(24) can be calculated explicitly. Straightforward calculations give

$$\frac{\partial\Sigma_\sigma(i\omega_n)}{\partial W_{\alpha s}} = \frac{1}{(Z(i\omega_n) + \sigma s J_H - \alpha U)A_\Sigma(i\omega_n)}, \quad (25)$$

$$\frac{\partial\Sigma(i\omega_n)}{\partial G(i\omega_n)} = -\frac{A_G(i\omega_n)}{A_\Sigma(i\omega_n)}, \quad (26)$$

$$\frac{\partial W_{\alpha s}}{\partial Z_\sigma(i\omega_n)} = \frac{W_{\alpha s}}{Z(i\omega_n) + \sigma s J_H - \alpha U} - W_{\alpha s}G(i\omega_n), \quad (27)$$

where

$$\begin{aligned} A_\Sigma(i\omega_n) &= \sum_{\alpha s}\frac{W_{\alpha s}}{(Z(i\omega_n) + \sigma s J_H - \alpha U)^2}, \\ A_G(i\omega_n) &= -\sum_{\alpha s}W_{\alpha s}\frac{G^{-1}(i\omega_n)}{(Z(i\omega_n) + \sigma s J_H - \alpha U)^2}[Z(i\omega_n) + \sigma s J_H - \alpha U - G^{-1}(i\omega_n)]. \end{aligned}$$

In such the way, Eqs. (19)-(24) fully determine the susceptibilities, once the self-consistent equations of the DMFT are solved. The charge or spin correlation function diverges whenever $\hat{\gamma}(\mathbf{q})$ diverges, which happens when the determinant

of $\hat{Q}(\mathbf{q})$ vanishes. The divergence indicates the instability of the disordered paramagnetic state. The \mathbf{q} dependence of the susceptibilities comes entirely from $\eta_n(\mathbf{q})$, and hence from the bare susceptibility $\chi_0(\mathbf{q}, i\omega_n)$. Within the DMFT^{16,22} in the infinite dimension limit all of the \mathbf{q} dependence of the bare susceptibility can be summarized in a single parameter $X = \sum_{\alpha=1}^d \cos q_{\alpha}/d$. One can show that^{16,22}

$$\chi_0(\mathbf{q}, i\omega_n) = \chi_0(X, i\omega_n) = -\frac{1}{\sqrt{1-X^2}} \int_{-\infty}^{+\infty} d\epsilon \frac{\rho(\epsilon)}{i\omega_n + \mu - \Sigma(i\omega_n) - \epsilon} F_{\infty} \left(\frac{i\omega_n + \mu - \Sigma(i\omega_n) - X\epsilon}{\sqrt{1-X^2}} \right),$$

where $F_{\infty}(z) = \int d\epsilon \rho(\epsilon)/(z - \epsilon)$ is used to denote the Hilbert transform. Now the instability of the disordered paramagnetic phase happens whenever the determinant of $\hat{Q}(X)$ vanishes at a certain value X . In particular, $X = -1$ corresponds to the checkerboard zone-boundary point $\mathbf{q} = (\pi, \pi, \dots, \pi)$ and the corresponding instability leads either to the charge checkerboard phase or to the antiferromagnetic phase at low temperature. $X = 1$ corresponds to the uniform zone center point $\mathbf{q} = 0$ and the corresponding instability leads to a charge segregation phase or FM phase at low temperature.

IV. NUMERICAL RESULTS

First, we consider the magnetic instability. In this case we calculate the spin correlation function as a function of X and temperature T . A divergence of the spin correlation function indicates a magnetic instability. For most values of J_H , U and n_e the spin correlation function diverges only at $X = 1$. In Fig. 1 we plot the typical behavior of the spin correlation function. The divergence of the spin correlation function at $X = 1$ indicates the FM stability. This means the FM state is established at low temperature. However for small values of J_H and n_e closed to 1, the spin correlation function also diverges at $X = -1$.^{30,31} This divergence indicates the stability of the antiferromagnetic phase at low temperature. In this paper we only consider the FM phase induced by the DE mechanism and its coexistence with CO phases. Thus in the rest of paper we consider the FM stability only. In Fig. 2 we present the FM transition temperature T_F as a function of U and n_e for various values of J_H . T_F is determined from the vanishing condition of the determinant of $\hat{Q}(X)$ at $X = 1$. Fig. 2(a) shows that the critical

temperature T_F decreases as increasing U and increases as increasing J_H . One expects in the limit $J_H \rightarrow \infty$ the FM transition temperature reaches its maximum value for fixed U . For fixed J_H the FM transition temperature is maximum if there is no JT distortion (i.e. $U = 0$). The JT distortion splits the energy level of Mn ions, and

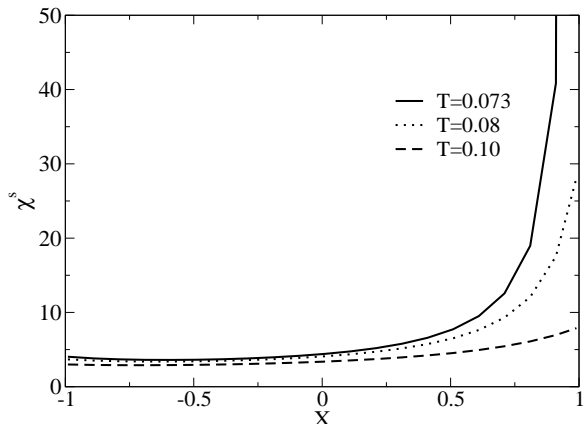


FIG. 1: The spin correlation function as a function of X at different temperatures ($n_e = 0.5$, $J_H = 2$, $U = 0.5$).

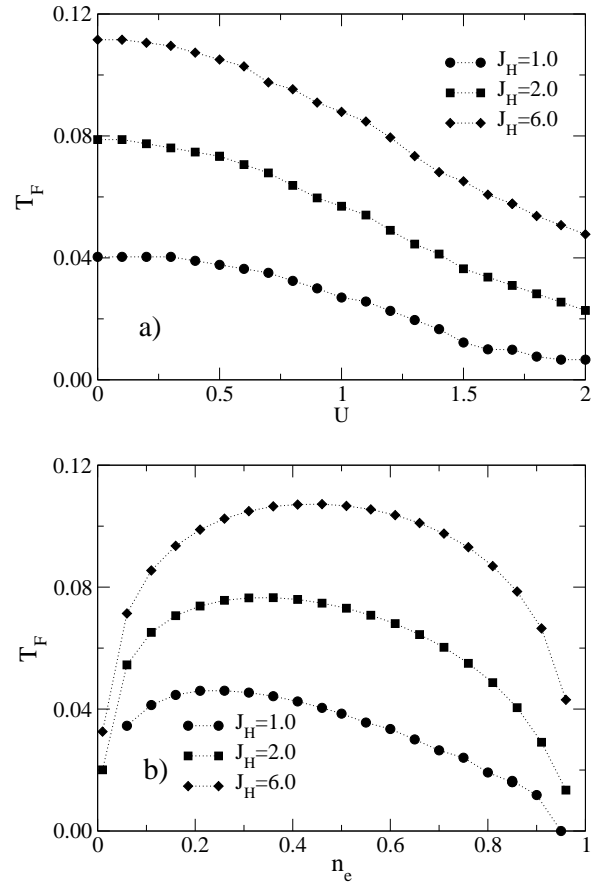


FIG. 2: The FM transition temperature T_F as a function of U [(a)] $n_e = 0.5$] and as a function of n_e [(b)] $U = 0.5$] for various values of J_H .

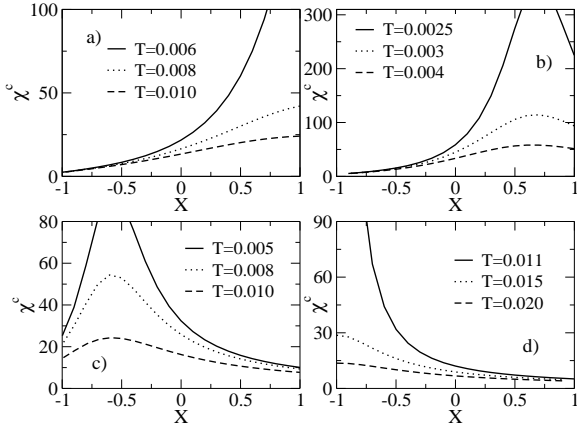


FIG. 3: The charge correlation function as a function of X at different temperatures. (a) $J_H = 0.1$, (b) $J_H = 0.2$, (c) $J_H = 0.4$, (d) $J_H = 0.5$. In all figures $U = 1.0$, $n_e = 0.6$.

this leads to suppress the FM transition temperature. This reduction of the FM transition temperature due to distortion is gradually significant already at intermediate values of U . In Figure 2(b) we also present the FM transition temperature as a function of doping n_e . In the limit $J_H \rightarrow \infty$, the FM transition temperature is maximum at half doping $n_e = 0.5$.²¹ However, for finite J_H its maximum shifts away from the half doping, to lower doping region.

Next, we consider the charge ordering instability. In this case, we study the divergence of the charge correlation function in the homogeneous paramagnetic phase. In Fig. 3 we plot the typical behaviors of the charge correlation function. They show that the charge correlation function may diverge at $X = 1$, $X = -1$ or at an intermediate value $-1 < X < 1$. The divergence at $X = -1$ indicates the checkerboard charge ordered state established at low temperature, while the divergence at $X = 1$ indicates the segregated state established at low temperature. The divergence at an intermediate value of X indicates the charge ordered phase being incommensurate at low temperature. The charge ordering critical temperature T_c is determined from the vanishing condition of the determinant of $\hat{Q}(X)$. However, one notices that for fixed values of J_H , U and n_e the determinant of $\hat{Q}(X)$ may vanish at different X and temperature T . Hence, we obtain the critical temperature $T_c(X)$ as a function of X . However, this does not indicate the stability of many charge ordered phases at low temperature. For certain values of J_H , U and n_e there is only one charge ordering transition which happens at the maximum temperature T_c among $T_c(X)$. Below this temperature T_c , although the charge correlation function may still diverge at other values of X , the divergence does not indicate a charge ordering, because the assumption of disordered phase is not valid anymore. Therefore the charge ordering critical temperature is determined not only from the vanishing

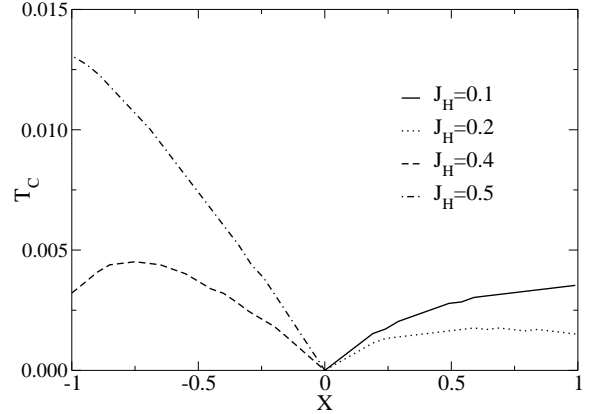


FIG. 4: The dependence of T_c on X in case of $U = 1.0$, $n_e = 0.6$ with various values of J_H .

condition of the determinant of $\hat{Q}(X)$, but also from the maximum condition¹⁶

$$T_c = \max_{\{X\}} T_c(X)$$

The corresponding value of X at which $T_c(X)$ is maximum determines the charge arrangement of the low temperature phase. In Fig. 4 we plot function $T_c(X)$ for different values of J_H . It shows that for fixed J_H , U , n_e we always find a unique maximum T_c . For small values of J_H we obtain the segregated state at low temperature. For large values of J_H the checkerboard ordered phase is observed. In an intermediate regime we also find an incommensurate charge ordering phase transition. In Fig. 5 we plot the charge ordering critical temperature as a function of U for various values of J_H . It shows that

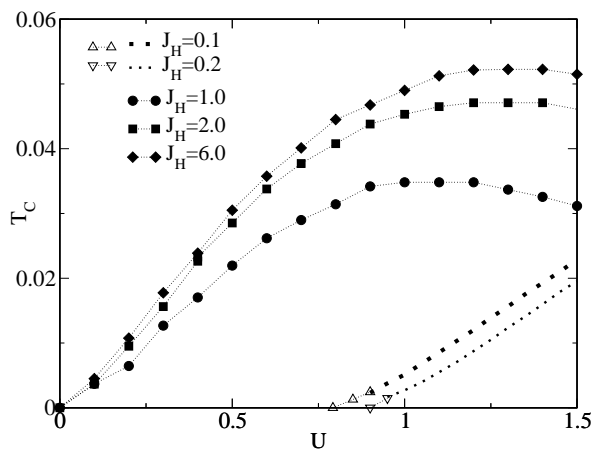


FIG. 5: The critical temperature of charge ordered phase transition as a function of U ($n_e = 0.5$). The filled (opened) symbols and the dotted lines correspond to the checkerboard (incommensurate) charge ordered phase and segregated phase, respectively.

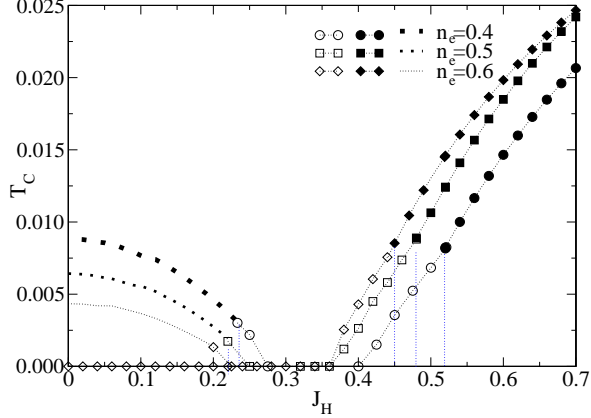


FIG. 6: The charge ordering critical temperature T_c as a function of J_H ($U = 1.0$). The filled (opened) symbols and the dotted lines correspond to the checkerboard (incommensurate) charge ordered phase and the segregated phase, respectively.

the checkerboard ordered phase is established for large values of J_H . As increasing U , the critical temperature first increases, reaches a maximum value, and then decreases. The behavior of the critical temperature is similar to the one obtained in the FK model.²⁹ For small values of J_H the checkerboard CO phase disappears and the segregated phase or incommensurate CO phase may be established depending on the value of U , as shown in Fig. 5. Figure. 5 also shows that the segregated phase is established at large values of U , while the incommensurate phase is established at smaller values of U . One notices that the segregated phase detected from the divergence of the charge correlation function constitutes a continuous phase transition. However, the phase transition is indeed first order.^{16,32} It can be shown by considering the free energy and using a Maxwell construction at low temperature.^{16,32} Usually, the critical temperature of the first order phase transition is higher than the one obtained from the divergence of the charge correlation function.^{16,32}

In Fig. 6 we plot the critical temperature T_c as a function of J_H for various doping n_e . It shows that the checkerboard charge ordered phase is established at large values of J_H and disappears at small J_H . Its critical temperature increases as increasing J_H . In contrast, the segregated phase is established at small values of J_H and its critical temperature decreases as increasing J_H . For intermediate values of J_H , both the checkerboard CO and segregated phases disappear, and an incommensurate CO phase is established. In Fig. 7 we plot the critical temperature T_c as a function of doping n_e for various values of J_H . For large values of J_H the checkerboard CO phase is established, and its critical temperature reaches maximum at half doping $n_e = 0.5$. For intermediate values of J_H , the CO phase is established at large doping $n_e > 0.5$, and disappears at smaller doping. Instead of the checker-

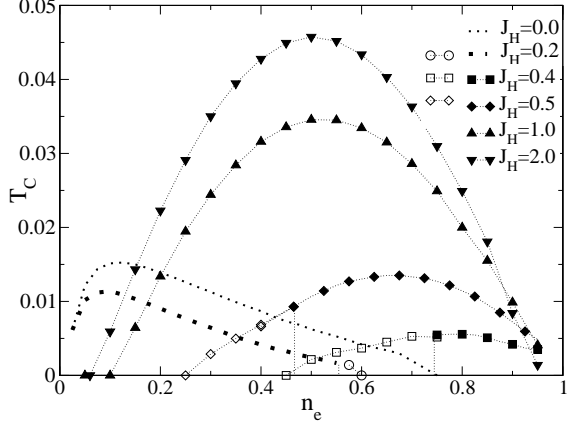


FIG. 7: The charge ordering critical temperature T_c as a function of n_e ($U = 1.0$). The filled (opened) symbols and the dotted lines correspond to the checkerboard (incommensurate) charge ordered phase and the segregated phase, respectively.

board CO phase, an incommensurate phase appears. For small values of J_H only the segregated phase appears at small doping. At large doping the segregated phase also disappears.

We summarize the above results with the phase diagram in Fig. 8 which plots the regions of stability for different charge ordered phases. The stability is determined by the symmetry label X of the initial ordered phase as the temperature is lowered to the first instability at T_c . Furthermore, we assume that the symmetry label X of the ordered phase does not change as the temperature lowered from T_c to zero. Actually, the phase diagram is an approximation of the zero temperature phase diagram.¹⁶ The phase boundaries may change as one reduces the temperature from T_c to zero since the behaviors of incommensurate phases at low temperature are not able to be studied within the present approach. Moreover, the phase boundaries may also change if there are first-order phase transitions which may happen with the segregation phases. The phase diagram shows that the incommensurate phases is stabilized in buffer zones between the disordered and checkerboard CO phase or between the disordered and segregated phase. The segregated phase exists only for small values of J_H . For large values of J_H the checkerboard CO phase is stabilized. So far, we have obtained different charge ordered phases depending on the value of J_H , U and doping n_e . On the other hand, the system always exhibits the FM stability. Although the FM transition may happen first, in the FM phase the charge density still remains homogeneous and the charge correlation function is still normal as in the homogeneous paramagnetic phase. Hence one can use the charge instability signal in the high temperature homogeneous phase as the signal of charge ordering even if the system is already in the FM phase. Indeed, the charge ordering critical temperature detected from the charge order parameter in the CO-FM state coincides with the

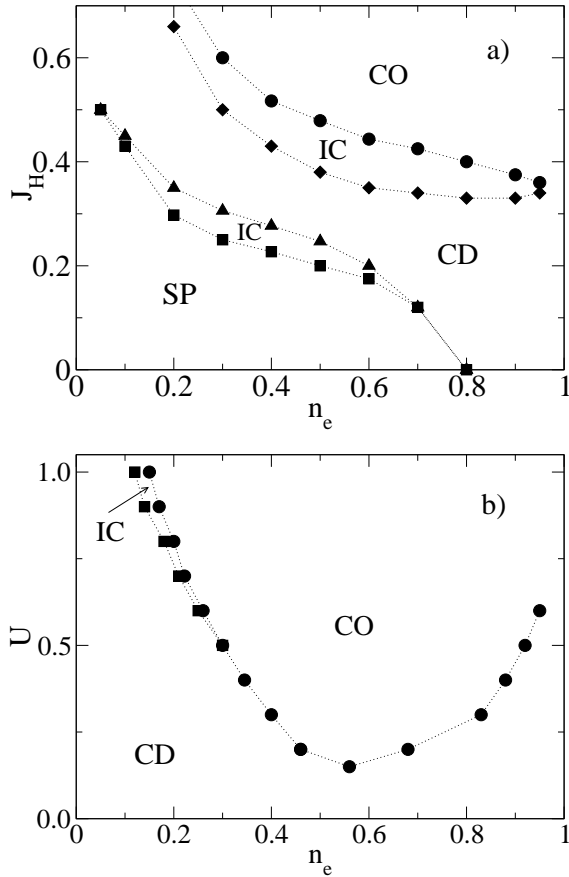


FIG. 8: Charge ordering phase diagrams: (a) $U = 1$; (b) $J_H = 1$. The shorthand CO denotes the checkerboard charge ordered phase; IC, the incommensurate phase; SP, the segregated phase, and CD, the charge disordered phase.

one calculated from the instability of the charge correlation function in the homogeneous paramagnetic phase.²¹ In such the way, the FM state coexists with different charge ordered phases for appropriate doping and distortion. One notices that in the previous studies^{31,33,34,35} a rich phase diagram which includes spin, charge and orbital ordered phases was also obtained. There is also a coexistence of the FM phase with checkerboard CO phase due to the Jahn-Teller phonons.^{31,33,34,35} In particular, the ferromagnetic CO phase is stabilized for large Jahn-Teller coupling and infinite Hund coupling. The conditions are in an agreement with the phase diagram in Fig. 8. However, in the previous studies^{31,33,34,35} only a phase separation between different magnetic phases was considered. A separation of charge ordered phases has not been addressed. In the present paper, a charge seg-

regated phase coexisting with the FM phase is obtained theoretically. The phase is a phase separated mixture of two types of Mn sites with different local geometric structures. The regime of the phase separation is particularly interesting, and possible consequences of its existence may be relevant to the experimental observations.⁸ However, the segregated phase appears only for weak Hund coupling and strong distortion. There is also a possible coexistence of the two segregated phases, one of which is between the magnetic phases, and the other is between the charge ordered phases. However, we leave the problem for further study.

V. CONCLUSION

In the present paper we have considered the doping and distortion effect on the double-exchange ferromagnetism. By employing the DMFT we have exactly calculated the charge and spin correlation function. A long range order is determined from the divergence signal of the correlation functions. The obtained results show that the system exhibits various phases which include the FM, checkerboard CO, incommensurate CO and segregated phases. In particular, the FM phase can coexist with the checkerboard CO phase for large values of J_H and with the segregated phase for small values of J_H . The incommensurate phases appear in the buffer zones between the regions of the charge ordered phases with different symmetries. It is interesting to note that experiments have observed both the CO-FM state⁵ and charge segregated phase.⁸ The phase separation between different charge ordered phases is a novel regime in manganites. By including the distortion effect in manganites via the Falicov-Kimball interaction we have simulated the charge segregated phase. The phase diagrams were found to clearly distinguish regions with robust CO-FM correlations and charge phase separation. However, manganites are too complicated of a system to be completely described by this simple model. In particular, experiments have observed inhomogeneous regions with different long-range orders.⁵ The study of the properties is beyond the capacity of the present method.

Acknowledgments

The authors grateful to Professor Jim Freericks for providing his papers and fruitful discussions. They also thank Professor Holger Fehske for valuable discussions. This work is supported by the National Program of Basic Research on Natural Science, Project 410104.

¹ M.B. Salamon and M. Jaime, Rev. Mod. Phys. **73**, 583 (2001).

² E. Dagotto, T. Hotta, and A. Moreo, Phys. Rep. **344**, 1 (2001).

³ C. Zener, Phys. Rev. **82**, 403 (1951).

⁴ N. Furukawa, J. Phys. Soc. Jpn. **63**, 3214 (1994); **64**, 2754 (1995); **65**, 1174 (1996).

⁵ J.C. Loudon, N.D. Mathur, and P.A. Midgley, Nature **420**, 797 (2002).

⁶ G. Subias, J. Garcia, M.G. Proietti, and J. Blasco, Phys. Rev. B **56**, 8183 (1997).

⁷ J. Garcia, M.C. Sanchez, G. Subias, and J. Blasco, J. Phys. Cond. Mat. **13**, 3229 (2001).

⁸ J. Herrero-Martin, J. Garcia, G. Subias, J. Blasco, and M. Concepcion Sanchez, Phys. Rev. B **70**, 024408 (2004).

⁹ F. Bridges, C. H. Booth, M. Anderson, G. H. Kwei, J. J. Neumeier, J. Snyder, J. Mitchell, J. S. Gardner, and E. Brosha, Phys. Rev. B **63**, 214405 (2001).

¹⁰ A. Daoud-Aladine, J. Rodriguez-Carvajal, L. Pinsard-Gaudart, M. T. Fernandez-Diaz, and A. Revcolevschi, Phys. Rev. Lett. **89**, 097205 (2002).

¹¹ V. Ferrari, M. Towler, and P.B. Littlewood, Phys. Rev. Lett. **91**, 227202 (2003).

¹² G. Zheng and C.H. Patterson, Phys. Rev. B **67**, 220404(R) (2003).

¹³ L.M. Falicov and J.C. Kimball, Phys. Rev. Lett. **22** 997 (1969).

¹⁴ V. Zlatic and J.K. Freericks, Acta Phys. Pol. B **34**, 931 (2003); **32**, 3253 (2001).

¹⁵ P. Farkasovsky, Phys. Rev. B. **51**, 1507 (1995).

¹⁶ J.K. Freericks and V. Zlatic, Rev. Mod. Phys. **75**, 1333 (2003).

¹⁷ J.K. Freericks and L.M. Falicov, Phys. Rev. B. **41**, 2163 (1990).

¹⁸ P. Lemberger, J. Phys. A **25**, 715 (1992).

¹⁹ G.I. Watson and R. Lemanski, J. Phys. Cond. Mat. **7**, 9521 (1995).

²⁰ J.K. Freericks and R. Lemanski, Phys. Rev. B **61**, 13438 (2000).

²¹ Tran Minh-Tien, Phys. Rev. B. **67**, 144404 (2003).

²² A. Georges, G. Kotliar, W. Krauth, and M.J. Rozenberg, Rev. Mod. Phys. **68**, 13 (1996).

²³ M.S. Laad, L. Craco, and E. Muller-Hartmann, Phys. Rev. B. **63**, 214419 (2001).

²⁴ V. Ferrari, M.J. Rozenberg, and R. Weht, Mod. Phys. Lett B **15**, 1031 (2001).

²⁵ T.V. Ramakrishnan, H. R. Krishnamurthy, S. R. Hassan, and G. Venketeswara Pai, Phys. Rev. Lett. **92**, 157203 (2004).

²⁶ W. Metzner and D. Vollhardt, Phys. Rev. Lett. **62**, 324 (1989).

²⁷ Phan Van-Nham and Tran Minh-Tien, Mod. Phys. Lett. B **17**, 39 (2003).

²⁸ B.M. Letfulov and J.K. Freericks, Phys. Rev. B **64**, 174409 (2001).

²⁹ U. Brandt and C. Mielsch, Z. Phys. B **75**, 365 (19869); **79**, 295 (1990); **82**, 37 (1991).

³⁰ B.M. Letfulov, Eur. Phys. J. B **14**, 19 (2000).

³¹ S. Yunoki, J. Hu, A. L. Malvezzi, A. Moreo, N. Furukawa, and E. Dagotto, Phys. Rev. Lett. **80**, 845 (1998).

³² J.K. Freericks, Ch. Gruber, and N. Macris, Phys. Rev. B **60**, 1617 (1999).

³³ S. Yunoki, T. Hotta, and E. Dagotto, Phys. Rev. Lett. **84** 3714 (2000).

³⁴ T. Hotta, A. L. Malvezzi, and E. Dagotto, Phys. Rev. B **62**, 9432 (2000).

³⁵ E. Dagotto, S. Yunoki, A. L. Malvezzi, A. Moreo, J. Hu, S. Capponi, D. Poilblanc, and N. Furukawa Phys. Rev. B **58**, 6414 (1998).